A Low-Cost, Open-Source, Robotic Airship for Education and Research

GAL GORJUP[ID]**, (Student Member, IEEE), AND MINAS LIAROKAPIS**[ID]**, (Senior Member, IEEE)**
New Dexterity research group, Department of Mechanical Engineering, The University of Auckland, Auckland 1010, New Zealand
Corresponding author: Gal Gorjup (ggor290@aucklanduni.ac.nz)

ABSTRACT Miniature indoor robotic airship platforms offer high mobility, safety, and extended flight times. This paper focuses on the feasibility, design, development, and evaluation of such a platform for robotics education and research. Selected commercially available envelope materials were considered and tested in terms of their helium retention capability and mechanical properties. The obtained envelope properties were used in a feasibility study, demonstrating that indoor airships are environmentally and financially viable, given an appropriate material choice. The platform's mechanical design was studied in terms of gondola placement and rotor angle positioning, resulting in an unconventional, asymmetric arrangement. The developed system was finally tested in a simple path following experiment for proof-of-concept purposes, proving its efficiency in attaining the desired heading and altitude configuration. The proposed robotic airship platform can be used for a variety of education and research oriented applications. Its design is open-source, facilitating replication by others.

INDEX TERMS Airship, lighter-than-air, open educational resources, path following, unmanned aerial vehicles.

I. INTRODUCTION

In the golden age of the giant airships, these vehicles had surpassed the fixed wing aircraft in terms of flight range, payload, and fuel efficiency. Even though the dream of filling the skies with fleets of transport and cargo ships has faded, the advantages of lighter-than-air (LTA) crafts remain. These can be applied in several fields of robotics education and research, where miniature robotic devices (both aerial and mobile) are slowly but surely making their appearance, attracting an increased interest.
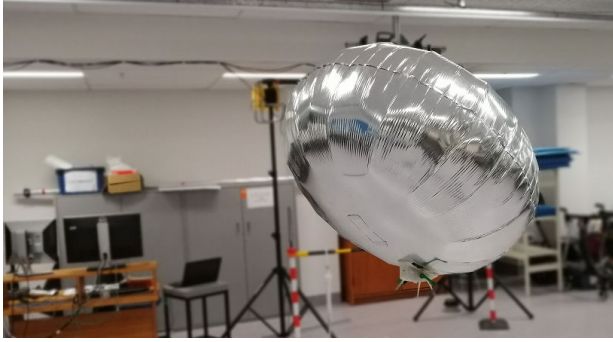
In terms of indoor exploration and navigation, airships offer higher mobility and looser path planning constraints when compared to ground robots. Additionally, their field of view is less obstructed and locomotion issues over different terrain and obstacles are bypassed completely. Conventional unmanned aerial vehicles (UAV) that are capable of static hovering in most cases generate lift purely through rotor thrust, which typically drains their battery in under 20 minutes. LTA vehicles, on the other hand, are able to maintain a desired altitude for significantly longer periods of time on a single battery charge [1]. In addition, airship platforms

The associate editor coordinating the review of this manuscript and approving it for publication was Zhenbao Liu[ID].

generally do not require precise collision control indoors, as their low speed and soft envelope prevent damage to themselves and their environment.

These attributes render LTA platforms an interesting solution for various robotics education and research applications. Even though their physical interaction capabilities are limited, their higher mobility and lower cost makes them a viable alternative to static or ground-based robots in many applications involving tele-embodiment, monitoring, guidance, and entertainment [2]–[5]. Compared to rotorcraft, airships are silent and safer due to the absence of sharp, high velocity rotor blades. This allows close proximity interaction and makes them more attractive to users [6].

Despite their promising features, the spread of indoor airship platforms is slow due to the design and control challenges they involve. The first task in LTA vehicle design is choosing an appropriate lifting gas. For indoor applications, helium is the default choice because of its non-reactive properties and high lift capabilities. Helium is non-renewable, making the choice of envelope material critical when considering environmental and financial aspects. Because of the small size of helium molecules, the gas escapes quickly through most conventional films which results in loss of lift over time. For indoor applications, the airship size is

FIGURE 1. The proposed low-cost, open-source, indoor robotic airship. The airship consists of a gondola containing all the electronics and rotors and a Qualatex Microfoil balloon (metallised PET).

also constrained by standard corridor and doorway widths, limiting their maximum lift and weight of mechanical and electronic components. Once built, an airship is hard to control due to its slow response times and nonlinear dynamics. This imposes some very nice problems in terms of control design from an educational perspective. Small crafts are also highly susceptible to external disturbances, as drafts and air conditioning may greatly influence the airship's behaviour.

This paper focuses on the feasibility, design, and development of an open-source, helium-based, indoor robotic airship that can be used for education and research purposes. First, this work focuses on the environmental and financial feasibility of the platform with respect to the helium losses through different envelope materials. The results offer yearly helium loss and related cost estimates for a range of commercially available balloons in an indoor environment. The mechanical properties of candidate materials are also evaluated. Then, the paper presents a compact gondola design and explores the effects of its placement and rotor angle positioning on flight stability. The efficiency of the final design is experimentally validated via a proof-of-concept path following exercise that proves its manoeuvring capabilities, while the airship's motion is being tracked by a Vicon motion capture system. Finally, the platform is examined in terms of cost and possible education and research applications are discussed.

The rest of this paper is organised as follows: Section II introduces the related work in the field, Section III presents the methods used, the analysis conducted, as well as the experimental setup, Section IV presents the obtained experimental results, Section V examines applications in research and education, while Section VI concludes the work and discusses future directions.

II. RELATED WORK

With the spread of intelligent robotic agents, numerous robotic platforms have been developed and disseminated in an open-source manner to allow replication by others in robotics education and research [7], [8]. Even though considerable progress has already been made in the field, most of the related work has focused on ground-based, stationary, or humanlike robotic devices [7], [9]–[11]. While they

are certainly a reasonable choice in many educational and research scenarios, such robots are often heavy, expensive, hard to replicate, or have limited mobility.

Such limitations can be overcome by indoor aerial platforms, which have in the recent years received a lot of attention. The most popular choice of such systems are quadrotors that have been developed as fully autonomous indoor, aerial robotic platforms [12]–[14]. Other studies have focused on indoor robotic airships. Skye [5] is a spherical omnidirectional blimp actuated by 4 rotors and equipped with a high resolution camera unit. It was intended for entertainment and interaction in large indoor and outdoor venues as the platform itself is quite large, with a diameter of 2.7 m. Another entertainment-oriented indoor airship platform is the Blimpduino [15], which features an Arduino-based control board that allows communication and basic control through a mobile app. The blimpduino came at a very affordable price of 90 USD, although it is not available for purchase anymore at the time of writing. A notable example of an autonomous indoor blimp is also the GT-MAB [16], one of the smallest autonomous indoor LTA platforms designed for human-robot interaction and autonomy studies. In [17], the GT-MAB was demonstrated in a human following and gesture recognition scheme, paving the road for flying airship companions.

Some research has also focused on human interaction with rotorcraft, where work was mainly based on one-directional communication through gesture recognition. In [18], the authors presented an agent capable of full-pose person tracking and accepting simple gestural commands. Authors of [19] expanded this concept by developing a gesture-based interface for communicating with teams of quadrotors. In [20], the authors reversed the information flow and examined the communication of UAV intent to a human user through motion. Regarding rotorcraft, only the visual mode of interaction was considered in human robot interaction research because these platforms are generally too loud for auditory communication and too dangerous for tactile communication. LTA vehicles, on the other hand, can be silent and harmless to the user, provided that an appropriate lifting gas is chosen.

The miniaturisation and democratisation of electronic components (access to sophisticated technology has become more accessible to more people) has allowed for progressively smaller and more low-cost designs of indoor airships, which have since become relevant for both robotics education and research. Initial studies have focused mainly on airship control and navigation, utilising the aerodynamic envelope shapes of their larger, outdoor airship counterparts. In [21], the authors presented an early indoor blimp system and studied visual servoing techniques. In [22], a dynamic airship model was developed and successfully applied in an indoor testing environment. Other examples that make use of the classic blimp envelope shapes include developments in blimp autonomy and navigation as described in [23], [24]. But all these studies have not focused on the feasibility of the robotic airship platforms, have not examined the permeability and

FIGURE 2. Evaluated balloons, from left to right: Qualatex untreated round 41 cm latex balloon, Qualatex untreated round 61 cm latex balloon, Qualatex round 61 cm latex balloon treated with UHF, Qualatex round 61 cm Bubble balloon and Qualatex round 91 cm Microfoil balloon.

applicability of different materials, the yearly helium losses, and the projected costs and none of these studies has proposed an open-source, platform that can be used for both robotics education and research.

III. METHODS

The lifting gas chosen for the proposed robotic airship platform is helium as it is safe and provides high lifting capacity. An alternative with comparable buoyancy is hydrogen, which was immediately discarded due to its high flammability characteristics. Hot air was also considered, but its lifting potential is significantly lower than that of the above gases. In addition, the heating element would pose a safety risk, especially for indoor use. Other lifting gas choices are either toxic, flammable or offer minimal buoyancy, making them inappropriate for this application.

A. ENVELOPE MATERIAL

Before designing the gondola, a number of envelope material candidates were examined with respect to their helium permeability and mechanical properties. To ensure a low cost platform, the envelope was chosen from the following set of commercially available balloons (see Figure 2):

- Qualatex untreated round 41 cm (16 inch) latex balloon
- Qualatex untreated round 61 cm (24 inch) latex balloon
- Qualatex round 61 cm (24 inch) latex balloon treated with Ultra Hi-Float (UHF) [25]
- Qualatex 61 cm (24 inch) clear Bubble balloon (layered membrane including a high barrier layer of ethylene vinyl alcohol copolymer)
- Qualatex round 91 cm (36 inch) Microfoil (metallised PET) balloon

To evaluate their helium permeability, the balloons' lifting capacities, along with their surfaces, were measured daily over the course of 16 days. Because of their elastic properties, the surfaces of latex and Bubble balloons were determined through their circumferences. The Microfoil balloon surface was measured before inflation as the material does not stretch. After collection, the helium escape rate was computed as the flux through the balloon envelope, given by:

$$J = \frac{\mathrm{d}Q}{\mathrm{d}t} \cdot \frac{1}{A} \qquad (1)$$

where J is the gas flux, Q is the amount of gas escaping, t is time and A is the envelope surface. The obtained helium escape rates were then averaged and used in a feasibility study projecting expected helium losses through the membrane of an ideal spherical balloon. The approximate cost of helium used in the study was based on commercially available balloon gas tanks.

The mechanical properties of latex, Bubble and Microfoil materials were examined in terms of membrane thickness in the inflated state, membrane area density in the inflated state, membrane tensile strength, and membrane elongation characteristics. Material samples for latex were taken from the Qualatex untreated round 61 cm balloon. For the Microfoil balloon, thickness was measured in the uninflated state because the material stretching is negligible during inflation. As the latex and Bubble balloons stretch during inflation, their inflated membrane thickness t_i was estimated by assuming constant density of the material:

$$t_i = t_u \cdot \frac{A_u}{A_i} \qquad (2)$$

where t_u is the uninflated membrane thickness, A_u is the uninflated balloon surface, and A_i is the inflated balloon surface. The area density for all balloons was computed from the uninflated balloon mass and inflated balloon area. Material tensile strength and elongation were obtained experimentally, in accordance with the ASTM D412-16 Standard [26] for latex, and ASTM D882-18 Standard [27] for the Bubble and Microfoil materials. Samples were cut with the Standard Die C, as per ASTM D412-16 for all materials. The strain rate was 50 mm/min for Microfoil, and 500 mm/min for latex and Bubble samples. For each material, five samples were tested.

B. GONDOLA DESIGN AND PLACEMENT

The airship gondola was built around the chosen electronic components and actuators. The central control and communication unit is a Raspberry Pi Zero W running a Lite version of the Raspbian Stretch operating system. Peripheral components include a single cell 500 mAh Li-Ion battery, step-up voltage regulator, motor drivers, three 7×16 mm DC motors, three 57×20 mm propeller units and a camera module that will facilitate the formulation of HRI frameworks. Rotor speeds can either be controlled by on-board logic or manually via a wireless connection through SSH or an appropriately
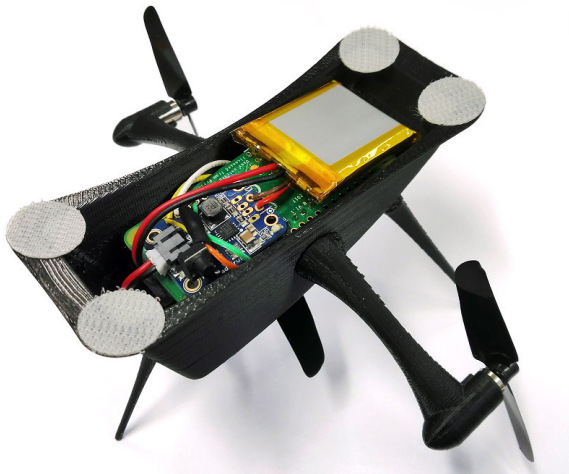
FIGURE 3. The assembled gondola of the robotic airship. All the electronics are located inside the gondola body and three rotors are used (see also Figure 4). The gondola is attached to the balloon through Velcro pads.


FIGURE 4. Exploded view of the robotic gondola. The electronics are depicted at the top of the figure, including the single cell Li-Ion battery. The camera is positioned in an angled configuration on the gondola and is depicted at the left of the figure. The modular rotor brackets and airship legs allow for easy replacement and fast modification.

developed Robot Operating System (ROS) package [28]. The combined cost of the gondola components (excluding the 3D printing filament and wiring) comes to 90 USD, which drops to 54 USD if the camera module is not required. Parameters for all subsystems of the robotic airship, including component descriptions, product codes, prices, and links to reseller webpages are collected in a bill of materials available through the website listed in Section VI.

The physical frame is 3D printed and built in a modular fashion: the gondola legs and rotor brackets were detachable to facilitate component modification and replacement. The assembled gondola and its exploded view model are presented in Figures 3 and 4, respectively. The gondola is attached to the chosen envelope using Velcro. The gondola
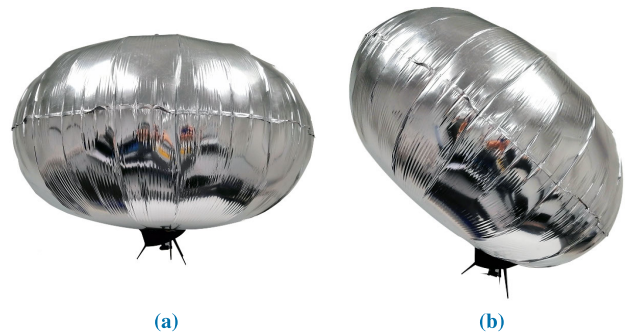
FIGURE 5. Centered (a) and angled (b) gondola positioning considered in the flight stability experiments.
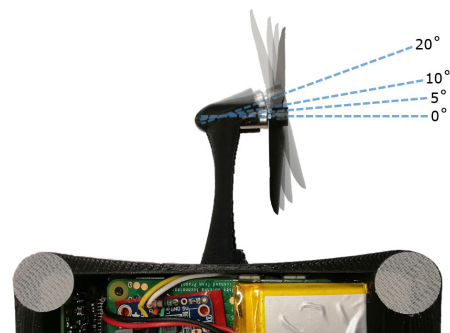
FIGURE 6. Side rotor angle configurations, with respect to the gondola axis of symmetry.

placement on the chosen envelope and the rotor angles with respect to the horizontal axis of gondola symmetry were determined experimentally to optimise flight stability. Two gondola placement options were considered. The first placement was centered and symmetric with respect to the envelope, in which case the side rotors were horizontal and a third one would in principle be required to control the airship altitude (Figure 5a). The second option angled the gondola with respect to the envelope centre, tilting the airship and shifting its side rotors out of the horizontal plane (Figure 5b). In this configuration, the airship orientation and altitude could be controlled using only the two side rotors. The side rotor angles of 0°, 5°, 10° and 20° were examined in the experiments. The four evaluated rotor angle configurations are depicted in Figure 6. The experiments consisted of 10 trials for each rotor angle and gondola placement at 25% and 50% of the rotor maximum speed (160 trials in total). The airship was released from a height of 1.5 m. During flight, the airship position and rotation were recorded with the Vicon motion optical capture system, which consists of 8 Vicon T-series cameras connected to the Giganet system. The Vicon Tracker software was used to capture the trajectories of reflective markers mounted on the airship envelope. The system sampling rate was 100 Hz.

C. PROOF-OF-CONCEPT PATH FOLLOWING
The airship was evaluated in terms of its path following ability in an indoor environment. The angled gondola placement

(Figure 5b) with 5° rotor angles was used in the experiments. Path following was implemented using a discrete variation of the carrot-chasing algorithm described in [29]. Because the two side rotors affected the airship's altitude in addition to its speed and heading, the algorithm was modified with a P controller that adjusted the baseline rotor speeds depending on the platform's current altitude.

---

Algorithm 1 Modified carrot-chasing path following
___
Input: (x, y, z), ψ, $W_{0...n} = [(x_0, y_0), \ldots (x_n, y_n)]$, N_t, z_t, P_ψ, P_z, C_{base}, C_{min}, C_{max},
Output: c_l, c_r
1: $i = \text{argmin}_i \|W_i - (x, y)\|$
2: $W_t = W_{i+N_t}$
3: $\psi_d = \text{atan2}(y_t - y, x_t - x)$
4: $\tilde{C}_{base} = C_{base} + P_z(z_t - z)$
5: $c_{l,r} = \tilde{C}_{base} \pm P_\psi (\psi_d - \psi)$
6: $c_{l,r} = \max(C_{min}, \min(C_{max}, c_{l,r}))$

The implemented computational flow of the modified carrot-chasing path following algorithm is presented in Method 1, where (x, y, z) is the current airship position, ψ is its heading (yaw) angle, $W_{0...n}$ is the desired path segmented into a sequence of equidistant waypoints, N_t is the look ahead index, z_t is the desired altitude, P_ψ and P_z are the heading and altitude gains, C_{base} is the default rotor control signal and C_{min}, C_{max} are the minimum and maximum allowed rotor values. The method outputs control signals for the left and right rotor c_l and c_r. The proposed airship relies on two rotors for both altitude and heading control for simplicity reasons. This choice imposes certain instability to the platform. Multiple basic control methods that are typically used in undergraduate Engineering courses were examined and a basic proportional control provided the best results in terms of path tracking efficiency and simplicity. Other, more sophisticated methods can also be used, which is a matter of future research from users of the proposed device. The framework was implemented as a collection of nodes within the ROS architecture, which provided the basic communication utilities and allowed for easy debugging. The airship real time position and orientation were continuously published by a node tracking the airship, which was connected to the Vicon data stream. It ran on a personal computer, along with a node running the path following algorithm and publishing the rotor control signals with a rate of 5 Hz. The airship was running a single node that was receiving the control signals and setting the desired rotor speeds. For this application, the path following and rotor control nodes were written in Python. The airship node running on the Raspberry Pi Zero was communicating with the rest of the system through Wi-Fi, on a dedicated local network. The associated communication latency was in the range of approximately 3 ms, which has proven to be sufficiently low for the proposed application. The system was tested on a circular path with a diameter of 4 m and waypoint spacing of 10 cm. The target altitude z_t was set to 1.8 m,
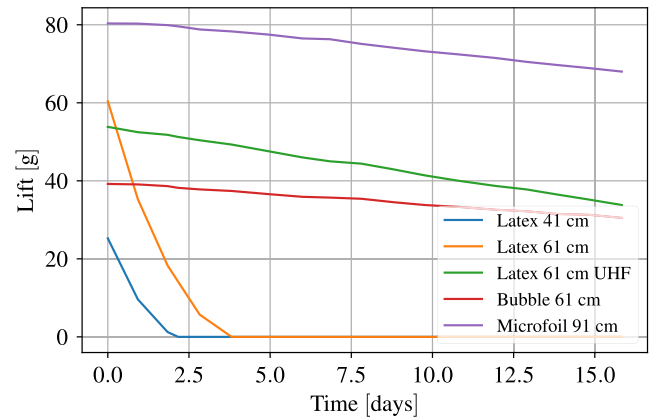
FIGURE 7. Measurements focusing on balloon lift over time. As it can be noticed, the untreated latex balloons experienced a rapid decrease in the available lift, while the Bubble and Microfoil provided the best results.

with a gain of $P_z = 25$. The base rotor control signal was set to $C_{base} = 53$ on a scale of 0 to 255, while C_{min} and C_{max} were set to 30 and 255, respectively. The look ahead index N_t and heading gain P_ψ were manually tuned with the goal of minimising the cross-track error. Position and orientation of the airship during path following was recorded and examined.

IV. RESULTS
A. ENVELOPE

From the raw balloon lift measurements (Figure 7), it is visible that the untreated latex balloons lost their lifting ability in a matter of days, while others were deflating linearly at a much slower rate. A more direct material comparison was possible through determining the helium flux through the balloon membranes. To accommodate the experimental data, (1) was converted into an approximate, discrete form:

$$J = \frac{\Delta Q}{\Delta t} \cdot \frac{1}{A}, \tag{3}$$

where ΔQ was computed from the daily lift loss and Δt was the time between measurements. The amount of gas escaping Q was defined as the volume of helium at standard temperature and pressure (STP), according to IUPAC which defines them as $T_{STP} = 273.15$ K and $p_{STP} = 10^5$ Pa [30]. Assuming that helium behaves like an ideal gas, the actual escaped gas volume V_a can be converted into V_{STP} according to the ideal gas law:

$$V_{STP} = V_a \cdot \frac{p_a}{p_{STP}} \cdot \frac{T_{STP}}{T_a} \tag{4}$$

Because the balloons were kept in a laboratory environment at sea level, the actual pressure and temperature were assumed constant at $p_a = 101.325$ kPa and $T_a = 293.15$ K. Assuming the pressure difference on the balloon membrane was negligible, the helium lifting capacity l_{He} in the laboratory environment was computed as:

$$l_{He} = \frac{m}{V_a}, \tag{5}$$

TABLE 1. Average helium flux values and yearly refill cost projections for helium lost through the membrane of spherical balloons of different types with diameters of 60 cm and helium gas price of 150 USD/m^3_{STP} (as of 20.1.2020).

Balloon Type	Average He Flux $[\frac{m^3_{STP}}{day \cdot m^2}]$	Daily He Loss $[m^3_{STP}]$	Yearly He Loss $[m^3_{STP}]$	Yearly Refill Cost [USD]
Latex	0.0270	0.0305	11.1	1665
UHF Latex	0.00146	0.00165	0.602	90
Bubble	0.000757	0.000855	0.312	47
Microfoil	0.000641	0.000724	0.264	40
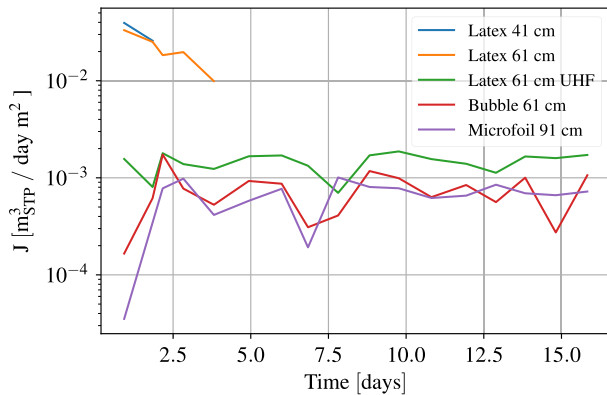
FIGURE 8. Daily helium flux through the balloon membranes. The two untreated latex balloons deflated after 2 and 4 days. The Bubble and Microfoil balloons provided the best helium retention capabilities.

where m is the lifted mass and V_a is the helium volume at laboratory conditions. The l_{He} for the used balloon grade helium was experimentally determined to be 0.95 $\frac{kg}{m^3}$ from the latex balloon volumes, lifts and masses. Combining the above, the daily helium escape flux through the balloon membranes was computed (Figure 8).

Examining the obtained results, it is immediately visible that untreated latex is the least appropriate for an airship application. The helium was lost through the porous material in a matter of days and latex itself ages with time and UV exposure. Latex treated with UHF exhibits substantially better helium retention properties, comparable to those of the Bubble and Microfoil balloon materials. However, even UHF treated latex is subject to aging and easily bursts on impact with a rough surface. The Bubble and Microfoil balloons performed equally well in terms of helium retention, although an issue with Bubble balloons is their availability in terms of different sizes. For the experiments, the largest available Bubble size was selected and it could only lift 40 g at maximum inflation. While this might be enough for an optimised solution, it did not suffice in the prototyping stage. The helium escape flux measurements were averaged over the experiment period and collected in Table 1, where values for untreated latex balloons were merged. The table also presents the daily and yearly helium losses through the membrane of a spherical balloon that has a diameter of 60 cm corresponding to a surface of $A = 1.13$ m². The flux values in the first row present the helium loss per day and per square meter,

while the daily and yearly rates demonstrate the actual helium loss through the balloon membrane. Using approximate retail balloon gas costs, the yearly expenses of compensating the lost helium were computed (note that the yearly costs do not include the initial cost of filling the balloon, which is 16.5 USD). Examining these yearly cost projections, it is evident that helium related maintenance of an indoor airship is cheap, given an appropriate choice of envelope material. Such platforms are thus feasible from an environmental and financial standpoint.
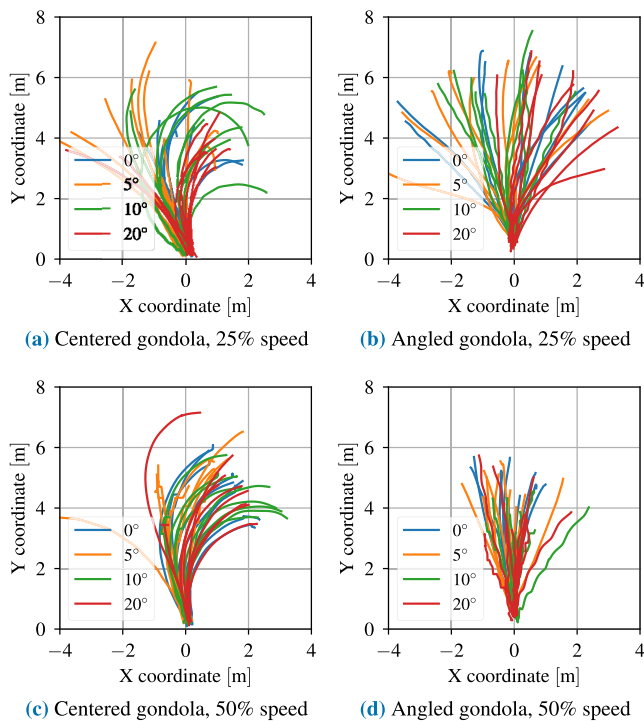
Concerning the mechanical properties of evaluated materials (Table 2), the bubble balloon stands out with a roughly 20% lower area density, which converts to a higher payload for equal envelope volumes. The latex balloon was found to have a comparably low tensile strength, as well as an elongation of over 800 %, which is due to the material's considerable thickness in the uninflated state. The Microfoil material was measured to have highest tensile strength with minimal spread, as well as a comparably low elongation. Since the proposed platform is not intended for high altitude operation, the envelope does not need to withstand extreme pressure and temperature changes. Instead, the critical material characteristic is its area density, which greatly influences the payload in cases where size is a hard constraint. From a mechanical aspect, the Bubble material would thus be most appropriate, with lowest area density and suitable material strength. However, the maximum achievable payload with a commercially available Bubble balloon is too low (40 g), and manufacturing custom envelopes would significantly increase the platform cost and reduce accessibility. The chosen envelope for this application was therefore the 90 cm Microfoil balloon, with excellent helium retention capabilities, high enough payload, and appropriate material strength characteristics.
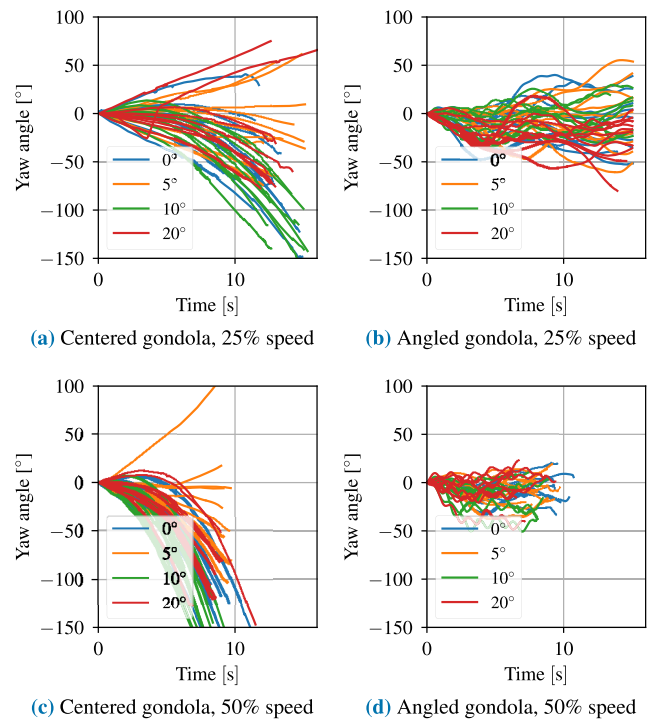
B. GONDOLA PLACEMENT AND ROTOR ANGLES
The experiment results are presented in terms of the airship horizontal XY position (Figure 9) and its yaw (Figure 10) during flight. Examining the figures, it is evident that the angled gondola offers greater flight stability than the centered option in the open loop. With the centered gondola, the airship tends to drift and turn right in most of the trials, which is even clearer at higher rotor speeds. With the angled gondola, airship flight is much more stable and its heading oscillates around a mean value instead of diverging.

TABLE 2. Mechanical properties of the evaluated latex, Bubble, and Microfoil balloon membrane materials.

Membrane Material	Thickness (Inflated) [μm]	Area Density (Inflated) [g/m^2]	Tensile Strength [MPa]		Elongation at Break [%]	
			Mean	Std. Dev.	Mean	Std. Dev.
Latex	24	25.3	25.1	3.46	824	22.27
Bubble	33	20.7	77.5	13.85	141	21.07
Microfoil	23	26.0	96.7	3.20	65	11.21

(a) Centered gondola, 25% speed

(b) Angled gondola, 25% speed

(c) Centered gondola, 50% speed

(d) Angled gondola, 50% speed

FIGURE 9. Open loop airship XY trajectories at different rotor angles for the centered and angled gondola configuration, at 25% and 50% rotor speed. It is evident that the angled configuration can better maintain the set course.

(a) Centered gondola, 25% speed

(b) Angled gondola, 25% speed

(c) Centered gondola, 50% speed

(d) Angled gondola, 50% speed

FIGURE 10. Open loop airship yaw at different rotor angles for the centered and angled gondola configuration, at 25% and 50% rotor speed. The yaw angles have been shifted to initialise at 0°. It is visible that the angled configuration is able to better maintain the set yaw angle, with minor oscillations.

Even though the drifting present in the centered gondola experiments is likely a result of unbalanced thrust in the open loop, it is still evident that the angled positioning is more robust to such disturbances. This increased robustness is likely a result of air flow dynamics around the asymmetric shape of the angled solution, although a dedicated aerodynamic analysis would be necessary to determine the exact cause. In addition to its disturbance robustness, the angled solution was interesting also because it allowed altitude and heading control using only the two side rotors, reducing the overall gondola weight. The varying rotor angles were not found to have a large impact on the overall airship behaviour in straight-line flight. However, in the case of the angled gondola, larger rotor angles tend to cause higher frequency oscillations of the yaw angle (Figure 10b and 10d). In addition, higher rotor angles seem less appropriate also because they waste a portion of their thrust negating each other.

C. PROOF-OF-CONCEPT PATH FOLLOWING

In this proof-of-concept application, the control parameters were found manually, as could be the case in basic design and control courses, where modelling and simulation are typically not part of the curriculum. Through the manual optimisation of the look ahead index and heading gain parameters presented in Section III-C, it was found that the values $N_t = 11$ and $P_\psi = 50$ produce a reasonably low cross-track error and stable path following behaviour (Figure 11a). As the distance between path waypoints was set to be 10 cm, the N_t value of 11 means that at every position on the path, the airship attempts to direct itself towards the waypoint that is 1.1 m ahead. The airship's altitude during path following exhibited some oscillations (Figure 11b), but there was no collision with either the floor or the ceiling of the motion capture laboratory. The recorded altitude is lower than the goal (1.8 m), which was expected considering the fact that it was regulated
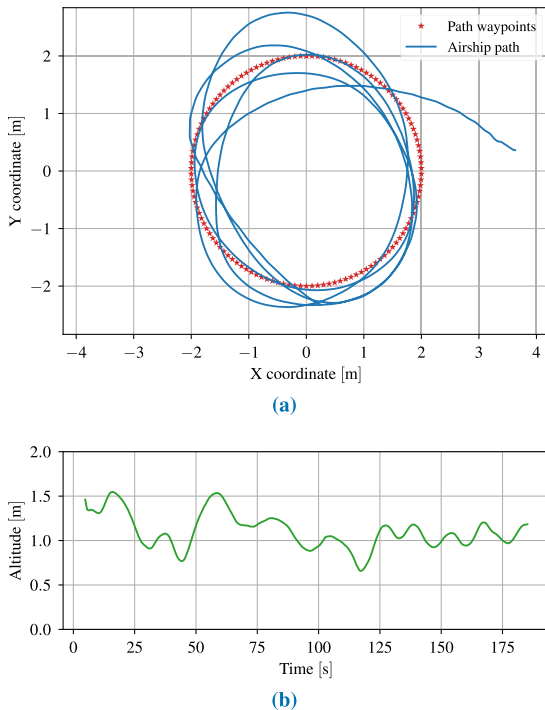
FIGURE 11. Airship path (a) and altitude (b) with look ahead index $N_t = 11$ and heading gain $P_\psi = 50$. It can be easily noticed that the airship can track the circular trajectory and maintain a constant altitude with some oscillations.

by means of a simple proportional controller. Overall, the path following experiments showed that simultaneous heading and altitude control using only the two rotors is indeed feasible. The results were not ideal in terms of cross-track error and oscillations in the airship altitude, but that is due to the fact that the chosen controller was not optimal for this setting and its parameters were determined manually. This experiment was conducted for proof-of-concept educational purposes.

V. APPLICATIONS
As discussed in Section III-B, the developed platform has a cost of 90 USD. If we include also the recommended balloon type (4 USD) and the initial filling cost (16.5 USD), the total cost of the airship comes to 110.5 USD. This is comparable to alternative indoor blimp kits, such as the Blimpduino 2.0 [15], which costs 90 USD. The Blimpduino kit, however, features a simple microcontroller that is less flexible than the single-board computer integrated into the proposed platform. Considering also the camera module, the open-source gondola design, the ROS compatibility, and the sample closed-loop control scheme, the proposed platform is much better suited for research and education purposes.

Concerning educational use, the platform can be easily incorporated into science and engineering courses on the secondary or tertiary level. For a mechanically-oriented curriculum, the students can work on gondola design and weight optimisation, developing their CAD and rapid prototyping skills. The airship is also ideal for control courses, where the students can develop and apply controllers that range from

basic PID to complex, model-based control. An advantage of using a single-board computer as the core control component is also that the code is not limited to a single programming language, since the airship can be controlled through the provided ROS interface, C/C++ or Python. Combining the above with assembly, wiring, and optional circuit design for motor drivers, the platform can be used as a complete mechatronics project that encompasses mechanics, electronics, and control.

For research, the small LTA platform is interesting in terms of controller development, as it is susceptible to drafts and ventilation that make reliable control difficult. Another opportunity is also in guidance and indoor exploration, where the challenge is to effectively utilise the limited computational power and simple RGB input to interpret its surroundings. Indoor exploration and navigation can be further examined in terms of micro-airship fleets. Such studies can build on [31], where the authors simulated the flight paths and collisions of several miniature airships with a similar shape and envelope type as those chosen in this work. Due to its safety and quiet operation, the platform can also be used in human-robot interaction studies. As the payload is limited, the challenge is to design a lightweight interface that can still effectively convey information and engage the user.

VI. CONCLUSION
This paper focused on the feasibility, design, development, and experimental evaluation of an open-source, helium-based, indoor robotic airship for robotics education and research. Several commercially available balloon materials were considered for the development of the airship envelope and they were evaluated in terms of their helium retention capability, as well as their mechanical properties. A cost projection based on the obtained material properties showed that indoor airships are environmentally and financially feasible. The effects of mechanical properties of the airship, including the gondola placement and rotor angles were examined, finding that an asymmetric placement yields higher flight stability than its symmetric counterpart. The airship was in the end shown to be capable of simultaneous path following and altitude control in a proof-of-concept experiment involving a Vicon optical motion capture system. All the airship designs, electronics, and code are disseminated in an open-source manner to allow replications by others. The files can be found at the following URL: http://www.newdexterity.org/openairship

REFERENCES
[1] D. Palossi, A. Gomez, S. Draskovic, A. Marongiu, L. Thiele, and L. Benini, "Extending the lifetime of nano-blimps via dynamic motor control," *J. Signal Process. Syst.*, vol. 91, nos. 3–4, pp. 339–361, Mar. 2019.

[2] E. Paulos and J. Canny, "PRoP: Personal roving presence," in *Proc. CHI*. New York, NY, USA: ACM, 1998, pp. 296–303.

[3] H. Tobita and T. Kuzi, "Face-to-avatar: Augmented face-to-face communication with aerotop telepresence system," in *Proc. Int. Work. Conf. Adv. Vis. Interface (AVI)*, 2012, pp. 262–265. [Online]. Available: http://dl.acm.org/citation.cfm?id=2254605

[4] S. Oh, S. Kang, K. Lee, S. Ahn, and E. Kim, "Flying display: Autonomous blimp with real-time visual tracking and image projection," in *Proc. IEEE/RSJ Int. Conf. Intell. Robots Syst.*, Oct. 2006, pp. 131–136.

[5] M. Burri, L. Gasser, M. Kach, M. Krebs, S. Laube, A. Ledergerber, D. Meier, R. Michaud, L. Mosimann, L. Muri, C. Ruch, A. Schaffner, N. Vuilliomenet, J. Weichart, K. Rudin, S. Leutenegger, J. Alonso-Mora, R. Siegwart, and P. Beardsley, "Design and control of a spherical omnidirectional blimp," in *Proc. IEEE/RSJ Int. Conf. Intell. Robots Syst.*, Nov. 2013, pp. 1873–1879.

[6] C. F. Liew and T. Yairi, "Quadrotor or blimp? Noise and appearance considerations in designing social aerial robot," in *Proc. 8th ACM/IEEE Int. Conf. Hum.-Robot Interact. (HRI)*, Mar. 2013, pp. 183–184.

[7] S. S. Srinivasa, P. Lancaster, J. Michalove, M. Schmittle, C. Summers, M. Rockett, J. R. Smith, S. Choudhury, C. Mavrogiannis, and F. Sadeghi, "MuSHR: A low-cost, open-source robotic racecar for education and research," 2019, *arXiv:1908.08031*. [Online]. Available: http://arxiv.org/abs/1908.08031

[8] G. P. Kontoudis, M. V. Liarokapis, A. G. Zisimatos, C. I. Mavrogiannis, and K. J. Kyriakopoulos, "Open-source, anthropomorphic, underactuated robot hands with a selectively lockable differential mechanism: Towards affordable prostheses," in *Proc. IEEE/RSJ Int. Conf. Intell. Robots Syst. (IROS)*, Sep. 2015, pp. 5857–5862.

[9] M. Lapeyre, P. Rouanet, J. Grizou, S. N'Guyen, A. Le Falher, F. Depraetre, and P.-Y. Oudeyer, "Poppy: Open source 3D printed robot for experiments in developmental robotics," in *Proc. 4th Int. Conf. Develop. Learn. Epigenetic Robot.*, Oct. 2014, pp. 173–174.

[10] M. Kerzel, E. Strahl, S. Magg, N. Navarro-Guerrero, S. Heinrich, and S. Wermter, "NICO—Neuro-inspired companion: A developmental humanoid robot platform for multimodal interaction," in *Proc. 26th IEEE Int. Symp. Robot Hum. Interact. Commun. (RO-MAN)*, Aug./Sep. 2017, pp. 113–120.

[11] F. Arvin, J. Espinosa, B. Bird, A. West, S. Watson, and B. Lennox, "Mona: An affordable open-source mobile robot for education and research," *J. Intell. Robotic Syst.*, vol. 94, nos. 3–4, pp. 761–775, Jun. 2019, doi: 10.1007/s10846-018-0866-9.

[12] J. P. How, B. Behihke, A. Frank, D. Dale, and J. Vian, "Real-time indoor autonomous vehicle test environment," *IEEE Control Syst. Mag.*, vol. 28, no. 2, pp. 51–64, Apr. 2008.

[13] S. Grzonka, G. Grisetti, and W. Burgard, "A fully autonomous indoor quadrotor," *IEEE Trans. Robot.*, vol. 28, no. 1, pp. 90–100, Feb. 2012.

[14] T. Tomic, K. Schmid, P. Lutz, A. Domel, M. Kassecker, E. Mair, I. Grixa, F. Ruess, M. Suppa, and D. Burschka, "Toward a fully autonomous UAV: Research platform for indoor and outdoor urban search and rescue," *IEEE Robot. Autom. Mag.*, vol. 19, no. 3, pp. 46–56, Sep. 2012.

[15] *Blimpduino 2.0 Kit*. Accessed: Jan. 20, 2020. [Online]. Available: https://www.jjrobots.com/blimpduino-2/

[16] S. Cho, V. Mishra, Q. Tao, P. Vamell, M. King-Smith, A. Muni, W. Smallwood, and F. Zhang, "Autopilot design for a class of miniature autonomous blimps," in *Proc. IEEE Conf. Control Technol. Appl. (CCTA)*, Aug. 2017, pp. 841–846. [Online]. Available: http://ieeexplore.ieee.org/document/8062564/

[17] N. Yao, E. Anaya, Q. Tao, S. Cho, H. Zheng, and F. Zhang, "Monocular vision-based human following on miniature robotic blimp," in *Proc. IEEE Int. Conf. Robot. Autom. (ICRA)*, May 2017, pp. 3244–3249.

[18] T. Naseer, J. Sturm, and D. Cremers, "FollowMe: Person following and gesture recognition with a quadrocopter," in *Proc. IEEE/RSJ Int. Conf. Intell. Robots Syst.*, Nov. 2013, pp. 624–630.

[19] V. M. Monajjemi, J. Wawerla, R. Vaughan, and G. Mori, "HRI in the sky: Creating and commanding teams of UAVs with a vision-mediated gestural interface," in *Proc. IEEE/RSJ Int. Conf. Intell. Robots Syst.*, Nov. 2013, pp. 617–623.

[20] D. Szafir, B. Mutlu, and T. Fong, "Communication of intent in assistive free flyers," in *Proc. ACM/IEEE Int. Conf. Hum.-Robot Interact. (HRI)*, Mar. 2014, vol. 2, no. 1, pp. 358–365. [Online]. Available: http://dl.acm.org/citation.cfm?doid=2559636.2559672

[21] H. Zhang and J. P. Ostrowski, "Visual servoing with dynamics: Control of an unmanned blimp," in *Proc. IEEE Int. Conf. Robot. Autom.*, vol. 1, May 1999, pp. 618–623. [Online]. Available: http://ieeexplore.ieee.org/lpdocs/epic03/wrapper.htm?arnumber=770044

[22] J.-C. Zufferey, A. Guanella, A. Beyeler, and D. Floreano, "Flying over the reality gap: From simulated to real indoor airships," *Auto. Robots*, vol. 21, no. 3, pp. 243–254, Nov. 2006.

[23] P. González, W. Burgard, R. Sanz Domínguez, and J. López Fernández, "Developing a low-cost autonomous indoor blimp," *J. Phys. Agents*, vol. 3, no. 1, pp. 43–52, 2009.

[24] J. Muller, A. Rottmann, L. M. Reindl, and W. Burgard, "A probabilistic sonar sensor model for robust localization of a small-size blimp in indoor environments using a particle filter," in *Proc. IEEE Int. Conf. Robot. Autom.*, May 2009, pp. 3589–3594.

[25] H. K. Sinclair, "Gas barrier coating and coated elastomeric toy balloons," U.S. Patent 5 244 429 A, Sep. 14, 1993.

[26] *Standard Test Methods for Vulcanized Rubber and Thermoplastic Elastomers—Tension*, Standard ASTM D412-16, ASTM International, 2016.

[27] *Standard Test Method for Tensile Properties of Thin Plastic Sheeting*, Standard ASTM D882-18, ASTM International, 2018.

[28] M. Quigley, K. Conley, B. P. Gerkey, J. Faust, T. Foote, J. Leibs, R. Wheeler, and A. Y. Ng, "ROS: An open-source robot operating system," in *Proc. ICRA Workshop Open Source Softw.*, May 2009, p. 5.

[29] P. B. Sujit, S. Saripalli, and J. Borges Sousa, "Unmanned aerial vehicle path following: A survey and analysis of algorithms for fixed-wing unmanned aerial vehicless," *IEEE Control Syst. Mag.*, vol. 34, no. 1, pp. 42–59, Feb. 2014. [Online]. Available: http://ieeexplore.ieee.org/lpdocs/epic03/wrapper.htm?arnumber=6712082

[30] M. Nič, J. Jirát, B. Košata, A. Jenkins, and A. McNaught, *IUPAC Compendium of Chemical Terminology*, 2nd ed. Oxford, U.K.: Blackwell, 2009.

[31] B. Troub, B. DePineuil, and C. Montalvo, "Simulation analysis of a collision-tolerant micro-airship fleet," *Int. J. Micro Air Vehicles*, vol. 9, no. 4, pp. 297–305, Dec. 2017.

GAL GORJUP (Student Member, IEEE) was born in Trbovlje, Slovenia, in 1992. He received the B.S. degree in mechanical engineering from the University of Ljubljana, Slovenia, in 2014, and the M.S. degree in mechanical engineering from the University of Ljubljana, in collaboration with the University of Southern Denmark, in 2017. He is currently pursuing the Ph.D. degree in mechatronics engineering with The University of Auckland, New Zealand.

His research interests include human to robot skill transfer for grasping and dexterous manipulation tasks, with the goal of creating a robust and intuitive framework that will provide higher automation accessibility to a global user base. His awards include the 1st place of the Manufacturing track of the Robotic Grasping and Manipulation Competition of IEEE/RSJ International Conference on Robotics and Intelligent Systems (IROS) 2019 (Macau, China), and first prize for best presentation among 1st year PhD students participating in the 5th Mechanical Engineering Postgraduate Conference of The University of Auckland.

MINAS LIAROKAPIS (Senior Member, IEEE) received the Diploma degree in computer engineering from the University of Patras, Patras, Greece, the M.Sc. degree in information technologies in medicine and biology from the National Kapodistrian University of Athens, Athens, Greece, and the Ph.D. degree in mechanical engineering from the National Technical University of Athens, Athens.

He was a Postdoctoral Associate with the GRAB Lab, Yale University, USA. He is currently a Senior Lecturer with the Department of Mechanical Engineering, The University of Auckland, New Zealand, and a Research Advisor of the New Dexterity team. He is interested in providing robotics solutions to everyday life problems, modelling, designing and controlling novel robotics and bionics hardware. He is the founder of the OpenBionics initiative and a co-founder of OpenRobotHardware and HandCorpus.

● ● ●